Transition Metal Azolates from Metallocenes. 2. Synthesis, X-ray Structure, and Magnetic Properties of a Three-Dimensional Polymetallic Iron(II) Imidazolate Complex, a Low-Temperature Weak Ferromagnet

Steven J. Rettig, Alan Storr,* David A. Summers, Robert C. Thompson,* and James Trotter

Contribution from the Department of Chemistry, The University of British Columbia, Vancouver, BC, Canada, V6T 1Z1

Received May 13, 1997[⊗]

Abstract: The reaction of ferrocene with molten imidazole at 150 °C yielded pale yellow crystals of composition $[Fe_3(imid)_6(imidH)_2]_x$. Crystals of $[Fe_3(imid)_6(imidH)_2]_x$ are monoclinic, $a = 10.5912(9)$, $b = 12.958(2)$, $c = 10.617(1)$ Å; $\beta = 92.696(9)°$; $Z = 2$; space group $P2_1/c$. The structure was solved by Patterson methods and refined by full-matrix least-squares procedures to $R = 0.033$ and $R_w = 0.031$ for 2260 reflections with $I \geq 3\sigma(F^2)$. The structure consists of chains of tetrahedral iron centers cross-linked via octahedral iron ions to generate a 3-D array. All of the iron centers are bridged to four other metal centers via imidazolate ions, the two remaining (trans) coordination positions of the octahedral centers being occupied by neutral imidazole molecules. Magnetic susceptibilities on powdered samples were measured over the temperature range 2−300 K and at fields ranging from 0 to 55 000 G. The compound exhibits antiferromagnetic coupling along chains of tetrahedrally coordinated iron centers. A canted spin structure leads to weak ferromagnetism at temperatures below a magnetic phase transition temperature of 17 K. Upon cycling the applied magnetic field between +55 000 and −55 000 G at 4.8 K, a hysteresis loop was obtained with a remnant magnetization of 2500 cm^3 G mol^{-1} and a coercive field of 200 G.

Introduction

In our studies on transition metal azolate complexes[1−4] we have isolated a series of binary pyrazolates of copper(II) and cobalt(II). These compounds have polymeric structures which, as confirmed by X-ray studies on several copper(II) systems,[2a,b] consist of extended chains of metal ions doubly bridged by pyrazolate ligands. Magnetic studies on these polymeric compounds, as well as on some pyrazolate-bridged oligometallic systems, showed the pyrazolates to be relatively efficient mediators of magnetic exchange interactions. In extending this work to complexes of the 1,3-diazolate ligand imidazolate (imid), we anticipated that, as a bridging ligand, its π-delocalized nature should promote magnetic exchange interactions at least as strong as seen in the pyrazolate systems. Moreover, the 1,3-positioning of the donor nitrogens in the ligand should generate structures that are different from those seen in the pyrazolates. In particular, steric effects imposed by the CH groups in the 2-position of imidazolate make the double-bridging motif, which leads to 1-D chain polymers, unlikely. The possibility of forming extended structures of higher dimensionality with the imidazolate ligand makes structural and magnetic studies on these systems potentially very interesting.

Metal imidazolate complexes have been used in attempts to mimic active sites in metalloproteins due to the similarity of substituted imidazolate ligands and the histidine moiety at the metal binding sites of the proteins.[5,6] In addition to the biological interest, there have been a number of relevant studies reported in the literature on metal imidazolate complexes. In 1960, Jarvis and Wells[7] reported the 3-D structure for $[Cu(imid)_2]_x$. In 1964, the syntheses of binary metal imidazolates of nickel, copper, silver, and zinc were reported by Bauman and Wang.[8] Also in 1964, Brown and Aftergut described the preparation of bis(imidazolates) of copper, cobalt, and zinc.[9] Interestingly the $[Cu(imid)_2]_x$ complex isolated by Bauman and Wang was described as reddish-purple while the material prepared by Brown and Aftergut was blue. Inoue *et al.*[10] described the preparation of a third form (green) of $[Cu(imid)_2]_x$ in 1965 and reported on the temperature dependence of the magnetic susceptibilities of the three forms (green, brown, blue) in the following year.[11] In 1967, the structure of the zinc imidazolate, $[Zn(imid)_2]_x$,[12] was reported, and the structure of the cobalt analogue was published in 1975.[13] The structure of an imidazolato-bridged copper(II)−imidazole chloride polymeric complex, $[Cu(imid)(imidH)_2Cl]_x$, was detailed by Lundberg in 1972.[14] The material was determined to be comprised of chains of copper(II) ions linked by single imidazolate bridges. It has subsequently been shown to exhibit strong antiferromagnetic exchange.[15] In 1974, a single imidazolate-bridged polymer of

⊗ Abstract published in *Advance ACS Abstracts,* September 1, 1997.

(1) Rettig, S. J.; Storr, A.; Summers, D. A.; Thompson, R. C.; Trotter, J. *Can. J. Chem.*, in press.

(2) Ehlert, M. K.; Rettig, S. J.; Storr, A.; Thompson, R. C.; Trotter, J. *Can. J. Chem.* (a) **1989**, *67*, 1970−1974; (b) **1991**, *69*, 432−439; (c) **1992**, *70*, 2161−2173; (d) **1993**, *71*, 1425−1436.

(3) Ehlert, M. K.; Storr, A.; Thompson, R. C. *Can. J. Chem.* (a) **1992**, *70*, 1121−1128; (b) **1993**, *71*, 1412−1424.

(4) Ehlert, M. K.; Storr, A.; Summers, D. A.; Thompson, R. C. *Can. J. Chem.* **1997**, *75*, 491−498.

(5) Reed, C. A.; Landrum, J. T. *FEBS Lett.* **1979**, *106*, 265−267.

(6) Richardson, J. S.; Thomas, K. A.; Rubin, B. H.; Richardson D. C. *Proc. Natl. Acad. Sci. U.S.A.* **1975**, *72*, 1349−1353.

(7) Jarvis, J. A. J.; Wells, A. F. *Acta Crystallogr.* **1960**, *13*, 1027−1028.

(8) Bauman, J. E., Jr.; Wang, J. C. *Inorg. Chem.* **1964**, *3*, 368−373.

(9) Brown, G. P.; Aftergut, S. *J. Polym. Sci.* **1964**, *A2*, 1839−1845.

(10) Inoue, M.; Kishita, M; Kubo, M. *Inorg. Chem.* **1965**, *4*, 626.

(11) Inoue, M.; Kishita, M; Kubo, M. *Bull. Chem. Soc. Jpn.* **1966**, *39*, 1352.

(12) Freeman, H. C. *Adv. Protein Chem.* **1967**, *22*, 257−425.

(13) Strum, M.; Brandl, F.; Engel, D.; Hoppe, W. *Acta Crystallogr.* **1975**, *B31*, 2369−2378.

(14) Lundberg, B. K. S. *Acta Chem. Scand.* **1972**, *26*, 3902−3912.

S0002-7863(97)01558-8 CCC: $14.00

an iron(III) hemin was shown to possess unusual magnetic properties.[16] More recently, Chaudhuri *et al.* reported the structure and magnetic properties of an imidazolato-bridged trinuclear copper(II) complex.[17] The copper(II) ions in this compound form a triangular array, and antiferromagnetic coupling via the bridging ligands leads to uncompensated spin and so-called "spin frustration" behavior. Electrochemical syntheses and magnetic studies of a number of neutral transition metal imidazolates have also been reported recently.[18] In addition to the metal−imidazolate polymeric materials, there have been reported several oligometallic complexes in which imidazolate acts as a bridging ligand. Both homobimetallic and heterobimetallic imidazolate-bridged complexes have been described,[19−23] and magnetic studies on these systems[20,23] again reveal that the imidazolate linkage provides an efficient pathway for antiferromagnetic exchange. A series of 4(5)-substituted imidazolate-bridged bimetallic and trimetallic complexes has been thoroughly investigated by Matsumoto and others.[24−31] Again the results show the imidazolate linkage to promote magnetic exchange between paramagnetic metal centers.

In 1968, Seel and Sperber reported the synthesis, but no further characterization, of an iron(II) complex of composition $Fe(imid)_2 \cdot 0.5(imidH)$.[32] The present account utilizes imidazole (imidH) as a ligand precursor and describes the product obtained from the reaction of this azole with ferrocene. The polymer isolated here, $[Fe_3(imid)_6(imidH)_2]_x$, is a slightly different formulation from the one reported earlier for this reaction.[32] Characterization by X-ray crystallography reveals a structure incorporating both tetrahedral and octahedral Fe(II) centers linked in an extended three-dimensional array by bridging imidazolate ligands. Magnetic studies on powdered samples over the temperature range 2−300 K and at fields ranging from 0 to 55 000 G provide evidence for long-range magnetic ordering below 17 K and a net moment at low temperatures.

Experimental Section

Synthesis of $[Fe_3(imid)_6(imidH)_2]_x$. Ferrocene (0.50 g, 2.6 mmol) and imidazole (2.0 g, 26.0 mmol) were combined and sealed under vacuum in a Carius tube. The mixture was heated at 150 °C for 4 days. Over this period, the bright orange of the original solution of the ferrocene in molten imidazole (mp 90 °C) was discharged and pale yellow crystals deposited from the solution. The product and excess imidazole were allowed to cool to room temperature, and the Carius tube was opened under a dinitrogen atmosphere. The excess imidazole was extracted with dry and oxygen-free acetonitrile solvent, and the title compound was isolated as pale yellow crystals. Anal. Calcd for $Fe_3C_{24}H_{26}N_{16}$: C, 40.8; H, 3.7; N, 31.7. Found: C, 41.3; H, 3.5; N, 31.3.

Physical Measurements. Electronic spectra (200−3000 nm) were obtained using Nujol mulls pressed between quartz plates using a Varian Cary 5 UV−visible−near-IR spectrophotometer. Infrared spectra (4000−400 cm^{-1}) were recorded on a Bomen FTIR spectrophotometer. Samples were prepared as powders pressed between KBr plates.

Magnetic susceptibilities were measured using a Quantum Design (MPMS) SQUID magnetometer. The sample holder and procedures involving the use of the equipment were described previously.[2a] Magnetic susceptibilities were corrected for the background signal of the sample holder and for diamagnetic susceptibilities of all atoms (-460×10^{-6}). Susceptibility versus temperature behavior (2−300 K) was measured at 500 and 10 000 G. Magnetization versus applied field behavior (2−300 K) was measured at fields ranging from 0 to 55 000 G.

X-ray Crystallographic Analysis of $[Fe_3(imid)_6(imidH)_2]_x$. Crystallographic data for $[Fe_3(imid)_6(imidH)_2]_x$ appear in Table 1. The final unit cell parameters were obtained by least-squares fitting on the setting angles for 25 reflections with $2\theta = 27.4-34.3°$. The intensities of three standard reflections, measured every 200 reflections throughout the data collection, showed only small random fluctuations. The data were processed[33] and corrected for Lorentz and polarization effects and for absorption (empirical, based on azimuthal scans).

Table 1. Crystallographic Data[a]

compound	$[Fe_3(imid)_6(imidH)_2]_x$
formula	$C_{24}H_{26}Fe_3N_{16}$
fw	706.20
crystal system	monoclinic
space group	$P2_1/c$
a, Å	10.5912(9)
b, Å	12.958(2)
c, Å	10.617(1)
β, deg	92.696(9)
V, Å^3	1455.5(3)
Z	2 (formula units)
ρ_{calc}, g/cm^3	1.611
$F(000)$	720
radiation (λ, Å)	Mo (0.710 69)
μ, cm^{-1}	15.21
crystal size, mm	0.20 × 0.25 × 0.45
transmission factors	0.94−1.00
scan type	$\omega-2\theta$
scan range, deg in ω	1.15 + 0.35 tan θ
scan speed, deg/min	16 (up to eight rescans)
data collected	$+h, +k, \pm l$
$2\theta_{max}$, deg	60
crystal decay, %	negligible
total no. of reflections	4627
total no. of unique reflections	4413
R_{merge}	0.029
reflections with $I \geq 3\sigma(F^2)$	2260
no. of variables	196
R	0.033
R_w	0.031
gof	1.53
max Δ/σ (final cycle)	0.0003
residual density e/Å^3	−0.31 to 0.29

[a] Temperature 294 K, Rigaku AFC6S diffractometer, graphite monochromator, takeoff angle 6.0°, aperture 6.0 × 6.0 mm at a distance of 285 mm from the crystal, stationary background counts at each end of the scan (scan/background time ratio 2:1), $\sigma^2(F^2) = [S^2(C + 4B)]/Lp^2$ (S, scan rate; C, scan count; B, normalized background count), function minimized $\Sigma w(|F_o| - |F_c|)^2$, where $w = 4F_o^2/\sigma^2(F_o^2)$, $R = \Sigma||F_o| - |F_c||/\Sigma|F_o|$, $R_w = (\Sigma w(|F_o| - |F_c|)^2/\Sigma w|F_o|^2)^{1/2}$, and gof = $[\Sigma w(|F_o| - |F_c|)^2/(m - n)]^{1/2}$. Values given for R, R_w, and gof are based on those reflections with $I \geq 3\sigma(I)$.

(15) Bencini, A.; Benelli, C.; Gatteschi, D.; Zanchini, C. *Inorg. Chem.* **1986**, *25*, 398−400.
(16) Cohen, I. A.; Ostfeld, D. *ACS Symp. Ser.* **1974**, *No. 5*, 221−233.
(17) Chaudhuri, P; Karpenstein, I.; Winter, M.; Butzlaff, C.; Bill, E,; Trautwein, A. X.; Florke, U.; Haupt, H.-J. *J. Chem. Soc., Chem. Commun.* **1992**, 321−323.
(18) Vecchio-Sadus, A. M. *Transition Met. Chem.* **1995**, ***20***, 46−55.
(19) Costes, J. P.; Laurent, J. P. *Inorg. Chim. Acta* **1987**, *134*, 245−248.
(20) Costes, J. P.; Dahan, F.; Laurent, J. P. *Inorg. Chem.* **1991**, *30*, 1887−1892.
(21) Costes, J. P.; Serra, J. F.; Dahan, F.; Laurent, J. P. *Inorg. Chem.* **1986**, *25*, 2790−2795.
(22) Costes, J. P.; Fernandez-Garcia, M. I. *Inorg. Chim. Acta* **1990**, *173*, 247−254.
(23) Zong-Wan, M.; Qin-Wei, H.; Wen-Xia, T.; Shi-Xiaung, L.; Ze-Min, W.; Jin-Ling, H. *Polyhedron* **1995**, *15*, 321−325.
(24) Matsumoto, N.; Kanesaka, J.; Ohyoshi, A.; Nakamura, M.; Kohata. S.; Okawa, H. *Bull. Chem. Soc. Jpn.* **1987**, *60*, 3056−3058.
(25) Matsumoto, N.; Yamashita, S.; Ohyoshi, A. *J. Chem. Soc., Dalton Trans.* **1988**, 1943−1948.
(26) Matsumoto, N.; Maeda, Y.; Okawa, H.; Akui, T.; Kawaji, T.; Ohyoshi, A.; Kodera, M.; Oshio, H.; Kida, S. *J. Cham. Soc., Dalton Trans.* **1989**, 943−946.
(27) Matsumoto, N.; Okawa, H.; Kida, S.; Kawaji, T.; Ohyoshi, A. *Bull. Chem. Soc. Jpn.* **1989**, *62*, 3812−3816.
(28) Matsumoto, N.; Tamaki, H.; Inoue, K.; Koikawa, M.; Maeda, Y.; Okawa, H.; Kida, S. *Chem. Lett.* **1991**, 1393−1396.
(29) Matsumoto, N.; Inoue, K.; Ohba, N.; Okawa, H.; Kida, S. *Bull. Chem. Soc. Jpn.* **1992**, *65*, 2283−2285.
(30) Inoue, K.; Matsumoto, N.; Okawa, H. *Chem. Lett.* **1993**, 1433−1436.
(31) Matsumoto, N.; Nozaki, T.; Ushio, U.; Motoda, K.; Ohba, M.; Mago, G.; Okawa, H. *J. Chem. Soc., Dalton Trans.* **1993**, 2157−2162.
(32) Seel, F.; Sperber, V. *Angew Chem., Int. Ed Engl.* **1968**, *7*, 70.

Table 2. Bond Lengths (Å) with Estimated Standard Deviations (in Parentheses)[a]

bond	length	bond	length
Fe(1)−N(1)	2.183(2)	Fe(1)−N(3)	2.197(2)
Fe(1)−N(5)	2.253(3)	Fe(2)−N(2)	2.020(2)
Fe(2)−N(4)[a]	2.039(3)	Fe(2)−N(7)	2.046(3)
Fe(2)−N(8)[b]	2.053(2)	N(1)−C(1)	1.331(4)
N(1)−C(3)	1.369(4)	N(2)−C(1)	1.338(4)
N(2)−C(2)	1.385(4)	N(3)−C(4)	1.327(4)
N(3)−C(6)	1.365(4)	N(4)−C(4)	1.357(4)
N(4)−C(5)	1.375(4)	N(5)−C(7)	1.320(4)
N(5)−C(9)	1.371(4)	N(6)−C(7)	1.328(4)
N(6)−C(8)	1.363(4)	N(7)−C(10)	1.340(4)
N(7)−C(12)	1.373(4)	N(8)−C(10)	1.332(4)
N(8)−C(11)	1.371(4)	C(2)−C(3)	1.352(4)
C(5)−C(6)	1.363(4)	C(8)−C(9)	1.333(5)
C(11)−C(12)	1.355(4)		

[a] Superscript numbers refer to symmetry operations: (1) $-1 + x, y, z$. (2) $x, {}^1/_2 - y, -{}^1/_2 + z$.

Table 3. Bond Angles (deg) with Estimated Standard Deviations (in parentheses)

bonds	angle	bonds	angle
N(1)−Fe(1)−N(1)[3]	180.0	N(1)−Fe(1)−N(3)	91.82(9)
N(1)−Fe(1)−N(3)[3]	88.18(9)	N(1)−Fe(1)−N(5)	89.15(9)
N(1)−Fe(1)−N(5)[3]	90.85(9)	N(3)−Fe(1)−N(3)[3]	180.0
N(3)−Fe(1)−N(5)	88.59(10)	N(3)−Fe(1)−N(5)[3]	91.41(10)
N(5)−Fe(1)−N(5)[3]	180.0	N(2)−Fe(2)−N(4)[1]	128.0(1)
N(2)−Fe(2)−N(7)	104.8(1)	N(2)−Fe(2)−N(8)[2]	105.5(1)
N(4)[2]−Fe(2)−N(7)	99.3(1)	N(4)[2]−Fe(2)−N(8)[2]	103.58(10)
N(7)−Fe(2)−N(8)[2]	116.5(1)	Fe(1)−N(1)−C(1)	128.3(2)
Fe(1)−N(1)−C(3)	126.9(2)	C(1)−N(1)−C(3)	103.6(2)
Fe(2)−N(2)−C(1)	128.5(2)	Fe(2)−N(2)−C(2)	128.0(2)
C(1)−N(2)−C(2)	103.4(2)	Fe(1)−N(3)−C(4)	128.0(2)
Fe(1)−N(3)−C(6)	127.1(2)	C(4)−N(3)−C(6)	103.8(2)
Fe(2)[4]−N(4)−C(4)	125.4(2)	Fe(2)[4]−N(4)−C(5)	131.3(2)
C(4)−N(4)−C(5)	103.2(3)	Fe(1)−N(5)−C(7)	126.5(2)
Fe(1)−N(5)−C(9)	126.6(2)	C(7)−N(5)−C(9)	104.6(3)
C(7)−N(6)−C(8)	107.7(3)	Fe(2)−N(7)−C(10)	128.2(2)
Fe(2)−N(7)−C(12)	128.2(2)	C(10)−N(7)−C(12)	103.4(3)
Fe(2)[5]−N(8)−C(10)	130.1(2)	Fe(2)[5]−N(8)−C(11)	125.4(2)
C(10)−N(8)−C(11)	104.4(3)	N(1)−C(1)−N(2)	114.9(3)
N(2)−C(2)−C(3)	108.4(3)	N(1)−C(3)−C(2)	109.6(3)
N(3)−C(4)−N(4)	114.8(3)	N(4)−C(5)−C(6)	108.6(3)
N(3)−C(6)−C(5)	109.7(3)	N(5)−C(7)−N(6)	111.3(3)
N(6)−C(8)−C(9)	105.8(3)	N(5)−C(9)−C(8)	110.6(3)
N(7)−C(10)−N(8)	114.4(3)	N(8)−C(11)−C(12)	108.4(3)
N(7)−C(12)−C(11)	109.5(3)		

[a] Superscript numbers refer to symmetry operations: (1) $-1 + x, y, z$. (2) $x, {}^1/_2 - y, -{}^1/_2 + z$. (3) $1 - x, -y, -z$. (4) $1 + x, y, z$. (5) $x, {}^1/_2 - y, {}^1/_2 + z$.

The structure was solved by Patterson methods. The asymmetric unit contains two crystallographically independent iron atoms: one located at a center of symmetry and one in a general position. Non-hydrogen atoms were refined with anisotropic thermal parameters and hydrogen atoms were fixed in calculated positions with N−H = 0.91 Å, C−H = 0.98 Å, and $B_H = 1.2B_{\text{bonded atom}}$. No correction for secondary extinction was necessary. Neutral atom scattering factors for all atoms and anomalous dispersion corrections for the non-hydrogen atoms were taken from ref 34. Bond lengths and bond angles appear in Tables 2 and 3, respectively. Final atomic coordinates and equivalent isotropic thermal parameters, hydrogen atom parameters, anisotropic thermal parameters, torsion angles, non-bonded contacts and least-squares planes are included as Supporting Information.

Results and Discussion

The reaction of ferrocene with molten imidazole resulted in the deposition of a pale yellow crystalline material of empirical composition $Fe_3(imid)_6(imidH)_2$. The UV−visible−near-IR spectrum of the complex is shown in Figure 1 and displays two d−d absorption bands centered at 1265 and 1960 nm. These we assign to the ${}^5T_{2g} \rightarrow {}^5E_g$ transition for high-spin octahedral Fe(II) and to the ${}^5E \rightarrow {}^5T_2$ transition for tetrahedral Fe(II), respectively. The presence of these two types of metal centers was determined from an X-ray crystallographic study. The structure of the repeat unit in the polymer is shown in Figure 2, and the unit cell is shown in Figure 3. The structure reveals chains of tetrahedral iron centers cross-linked via octahedral iron ions. All of the iron centers are bridged to four other iron centers via imidazolate ions, the two remaining (trans) coordination positions of the octahedral centers being occupied by neutral imidazole molecules (IR ν_{N-H} 3380 cm^{-1}). The chains of tetrahedral iron ions are oriented along the *c* axis giving sheets of tetrahedral iron chains in the (100) plane. Each chain within

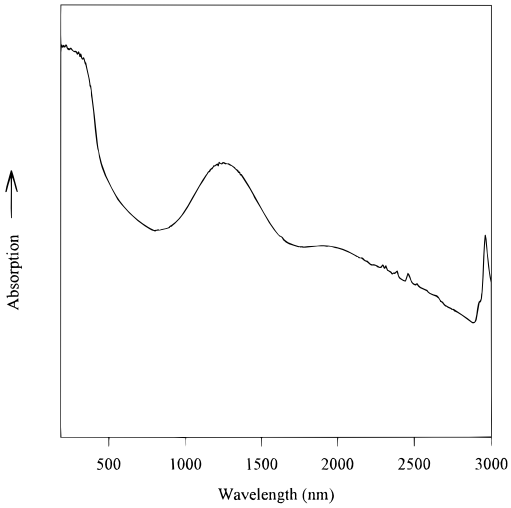

Figure 1. UV−visible-near-IR spectrum for $[Fe_3(imid)_6(imidH)_2]_x$. The sharp peak at 2950 nm results from the ν_{N-H} IR band (∼3380 cm^{-1}) and the sharp peaks at ∼2500 nm arise from the mulling agent, Nujol.

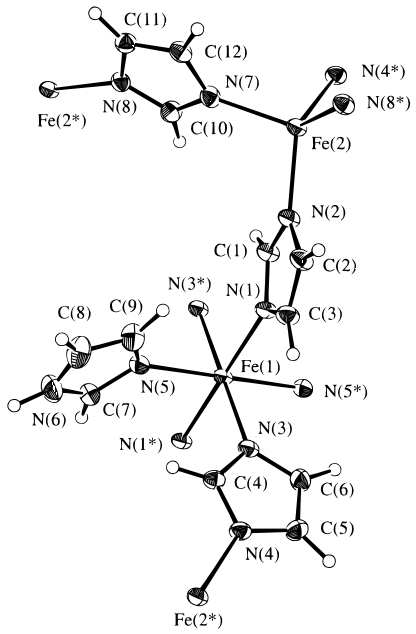

Figure 2. Molecular structure of the repeat unit of $[Fe_3(imid)_6(imidH)_2]_x$ with atom numbering scheme and 33% probability thermal elipsoids for all non-hydrogen atoms.

(33) *teXsan*: Structure Analysis Package. Molecular Structure Corp., The Woodlands, TX, 1995.

(34) (a) *International Tables for X-Ray Crystallography*; Kynoch Press: Birmingham, UK (present distributor, Kluwer Academic Publishers: Boston, MA) 1974; Vol. IV, pp 99−102. (b) *International Tables for Crystallography*; Kluwer Academic Publishers: Boston, MA, 1992; Vol. C, pp 200−206.

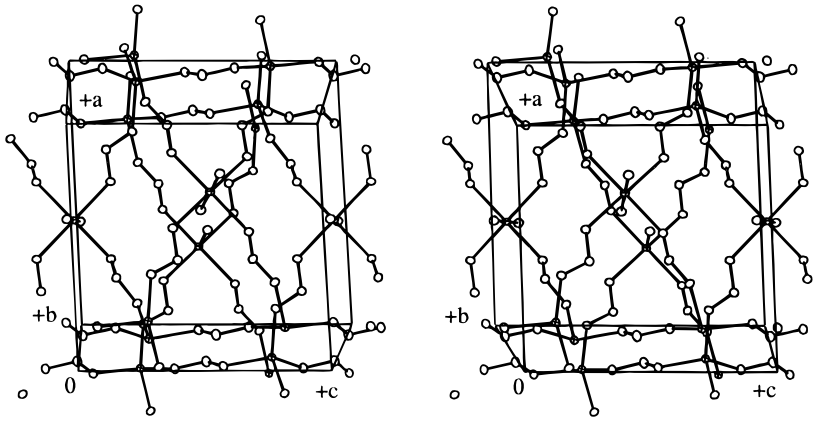

Figure 3. Stereoview of the unit cell of $[Fe_3(imid)_6(imidH)_2]_x$. For clarity, all hydrogen atoms, carbons 4 and 5 of imid, and all atoms except the coordinating nitrogen of imidH have been removed.

a sheet is linked via the octahedral irons to six different tetrahedral iron chains, two in each of the adjacent parallel sheets and two neighboring chains within its own sheet. The Fe−N bond distances around the octahedral Fe(1) are significantly longer at 2.183−2.253 Å than those around the tetrahedral Fe(2) at 2.020−2.053 Å. The angles N−Fe−N around octahedral Fe(1) are all close to 90° ranging from 88.18 to 91.82°; those around the distorted tetrahedral Fe(2) range widely from 99.3 to 128.0°.

The literature contains few references to structures of divalent transition metal imidazolate polymers, but the structures of $[Cu(imid)_2]_x$,[7] $[Zn(imid)_2]_x$,[12] and $[Co(imid)_2]_x$[13] have been reported. The $[Cu(imid)_2]_x$ structure, like the present structure, displays the metal ions in two distinct environments, in this case square planar and distorted tetrahedral. The $[Zn(imid)_2]_x$ and $[Co(imid)_2]_x$ structures have the metal(II) ions in a distorted tetrahedral environment. A common feature in the above three structures is the formation of $M_4(imid)_4$ rings that are cross-linked in the 3-D network with imidazolate bridges between the M(II) ions. In the present structure again we see large ring structures, in this case Fe_6imid_6 units, cross-linked into a 3-D network. This basic preference for larger metal ligand ring systems over the simple M_2L_2 rings of the metal(II) pyrazolate structures is readily understood on steric grounds. The adjacent donor N atoms of the pyrazolate ligands allow the formation of planar or boat like M−(N−N)$_2$−M six-membered rings in the extended $[Mpz_2]_x$ chain polymers.[1] With the imidazolate bridge, the donor N atoms are now separated by a C atom and M_2L_2 rings in the planar or boat like conformations required for a linear chain polymeric structure are sterically impossible. This M_2L_2 arrangement, however, was suggested recently, together with even more unlikely triply bridged M_2L_3 moieties as possible structural motifs in binary metal imidazolate systems.[18] Similar structural patterns have been documented with discrete molecular species in that $[Me_2Gapz]_2$ is dimeric with the Ga−(N−N)$_2$−Ga six-membered ring as the central feature;[35] whereas, $[Et_2Ga(2\text{-Meimid})]_4$ is tetrameric with the central feature being a $Ga_4(2\text{-Meimid})_4$ puckered ring system.[36]

The presence of linear chains of imidazolate-bridged tetrahedral iron ions in the 3-D network of the compound gives rise to the possibility of magnetic exchange between the paramagnetic metal centers in these chains. These chains of tetrahedral iron centers are cross-linked by imidazolate−octahedral iron−imidazolate bridges, which lead to an additional potential pathway for magnetic exchange. Magnetic susceptibility and χT versus T data on powdered samples of $Fe_3(imid)_6(imidH)_2]_x$ in an applied field of 500 G are shown in Figure 4. The results show an average magnetic moment which decreases from 5.48 to 3.74 μ_B (χT = 3.76 to χT = 1.75 cm^3 K mol^{-1}) with temperature decreasing from 300 to 17 K. There is a sharp upturn in the average moment to a maximum value of 14.3 μ_B (χT = 25.7 cm^3 K mol^{-1}; Figure 4) at 11 K. Magnetization versus applied field behavior is illustrated in Figure 5. Above 17 K, the magnetization varies linearly with applied field to the maximum field strength studied of 55 000 G. At temperatures below 17 K the magnetization no longer varies linearly with the applied field and a net magnetization of the compound is observed at zero field. The highest magnetization reached at 2 K and 55 000 G is 7280 cm^3 G mol^{-1}, significantly below the theoretical saturation magnetization of 22 300 cm^3 G mol^{-1}.[37] Upon cycling the field between +55 000 and −55 000 G at 4.8 K a hysteresis loop, the central portion of which is shown in Figure 6, is obtained with a remnant magnetization of 2500 cm^3 G mol^{-1} and a coercive field of 200 G.

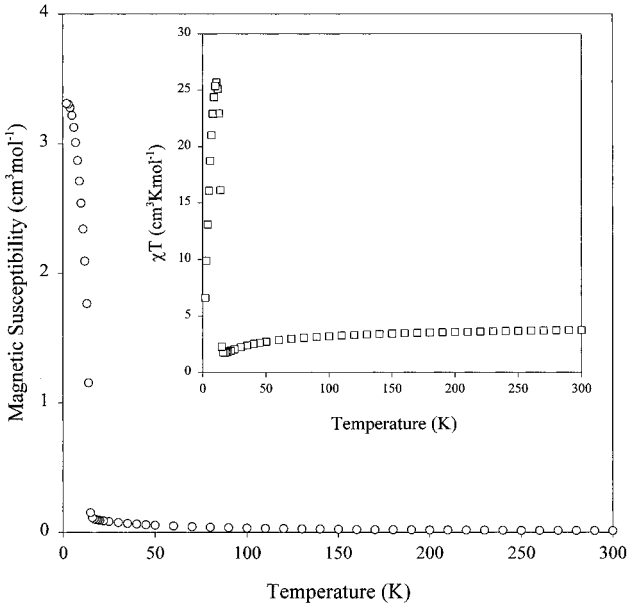

Figure 4. Magnetic susceptibility (○) and χT (□) versus temperature at 500 G for a powdered sample of $[Fe_3(imid)_6(imidH)_2]_x$.

In attempting to explain the magnetic behavior of this compound, we consider first the results obtained at temperatures

(35) Rendle, D. F.; Storr, A.; Trotter, J. *Can. J. Chem.* **1975**, *53*, 2930−2943.

(36) Breakell, K. R.; Rendle, D. F.; Storr, A.; Trotter, J. *J. Chem. Soc., Dalton Trans.* **1975**, 1584−1589.

(37) Carlin, R. L. *Magnetochemistry;* Springer-Verlag: Berlin, 1986; pp 7−9.

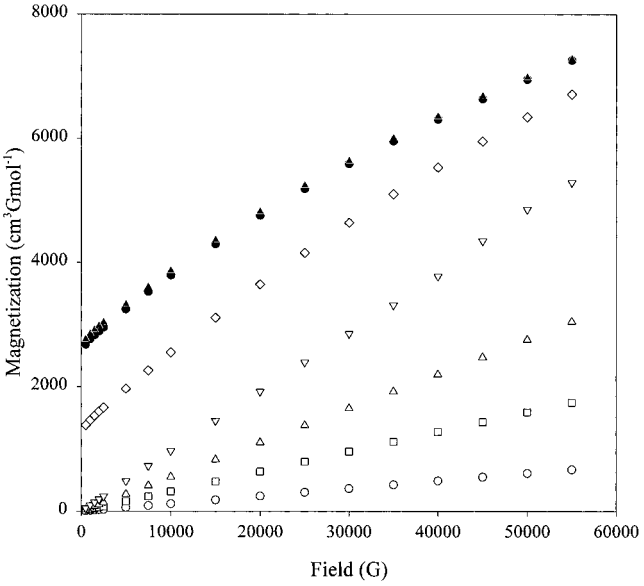

Figure 5. Magnetization versus applied magnetic field for $[Fe_3(imid)_6(imidH)_2]_x$ at 300 (○), 100 (□), 50 (△), 20 (▽), 13 (◇), 4.8 (●), and 2 K (▲).

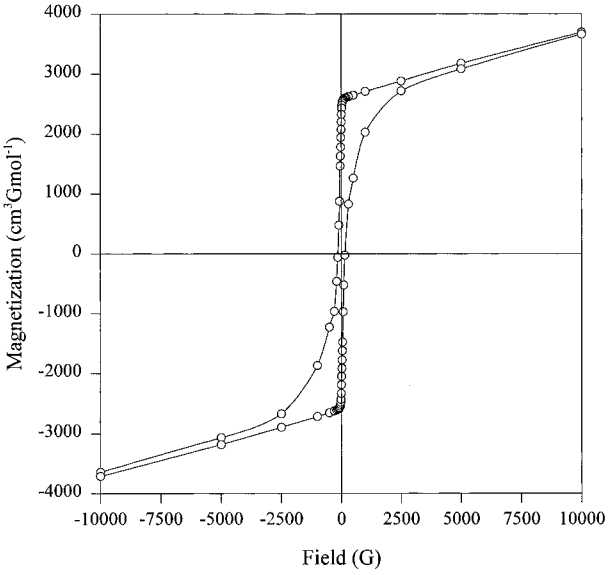

Figure 6. Field dependence of $[Fe_3(imid)_6(imidH)_2]_x$ at 4.8 K.

above 17 K. In the absence of magnetic exchange effects, the tetrahedral iron centers are expected to make a temperature-independent contribution to the magnetic moment while the octahedral centers, by virtue of the orbitally degenerate $^5T_{2g}$ ground state, are expected to make a temperature-dependent contribution.[38] The observed temperature-dependent moment behavior above 17 K may then be accounted for by single-ion effects associated with the octahedral metal centers combined, possibly, with antiferromagnetic exchange interactions in the lattice. A potentially very complicated modeling problem may be simplified by utilizing information available from the X-ray determined structure. The presence of unpaired electron density in both $e_{(g)}$- and $t_{2(g)}$-type metal orbitals in both T_d and O_h iron(II) centers suggests that orbital symmetry effects may not be important in determining whether exchange involving one metal type is stronger or weaker than that involving the other type. Metal to bridging-ligand bond strengths may, however, be important. The structure reveals that the Fe−N (bridge) bonds

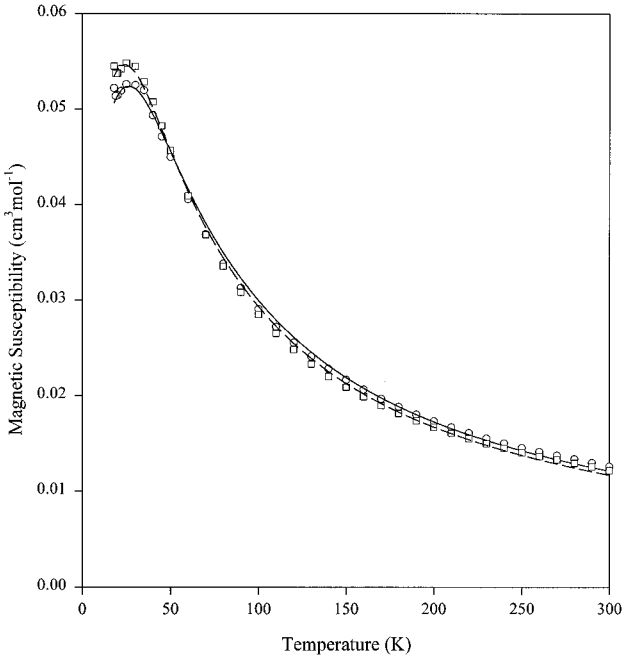

Figure 7. Plots of χ_{Fe}^{tet} versus temperature at 500 G. Magnetic contribution from χ_{Fe}^{oct} subtracted out as described in text for $\upsilon = 0$ (□) and $\upsilon = +10$ (○). The lines are calculated from theory as described in the text.

involving tetrahedral iron centers are significantly shorter than those involving the octahedral centers, suggesting that exchange interactions involving the tetrahedral iron should dominate. Accordingly, we modeled the magnetic susceptibility data above 17 K as arising from separate contributions from the different metal centers:

$$\chi_{Fe}^{exp} = (2/3)\chi_{Fe}^{tet} + (1/3)\chi_{Fe}^{oct} \quad (1)$$

Values of χ_{Fe}^{oct} (the susceptibility per mole of octahedral iron(II)) at different temperatures were interpolated from the theoretical data given by Figgis.[38] The theoretical values are given as functions of three parameters: (i) λ, the spin−orbit coupling constant; (ii) k, the orbital reduction factor, and (iii) υ, the axial distortion parameter. We chose two sets of parameters to model χ_{Fe}^{oct}. In both, k was fixed at 1 (no orbital reduction assumed) and λ was fixed at the free ion value for iron(II) of -100 cm^{-1}. In one set, υ was fixed at 0 (assumes no tetragonal distortion), and in the other, υ was fixed at $+10$. A positive value of υ is dictated by the X-ray structure, which shows an axial elongation. Negative υ parameters would apply to axial compression. The range of 0 to $+10$ represents the total range of distortion for which calculations were done in ref 38. From the measured susceptibilities (χ_{Fe}^{exp}) and these theoretical susceptibilities (χ_{Fe}^{oct}), values of χ_{Fe}^{tet} were then calculated from eq 1 and these data were plotted against temperature as shown in Figure 7. The results indicate antiferromagnetic interactions between tetrahedral iron centers. This interaction was analyzed by employing the model for linear chains of antiferromagnetically coupled $S = 2$ metal ions developed by Weng.[39] Hiller *et al.* generated eq 2, which reproduces

$$\chi_{chain} = \frac{Ng^2\mu_B{}^2(2 + 71.938x^2)}{(1 + 10.482x + 955.56x^3)kT} \quad (2)$$

Weng's numerical results,[40] and we have utilized this equation

(38) Figgis, B. N.; Lewis, J.; Mabbs, F. E.; Webb, G. A. *J. Chem. Soc. A* **1967**, 442−450.

(39) Weng, C. H. Ph.D. Thesis, Carnegie-Mellon University, Pittsburgh, PA, 1968.

to fit our experimental data. In eq 2, $x = |J|/kT$ and J is the exchange coupling constant. The best-fit values of g and J with υ set at 0 were 2.28 and -2.3 cm^{-1} ($F = 0.020$) while the best-fit values of g and J with υ set at $+10$ were 2.33 and -2.5 cm^{-1} ($F = 0.021$), respectively. The value of the fitting function, F, eq 3, was minimized in the fitting procedure. F

$$F = \left[\frac{1}{n}\sum_{i=1}^{n}\frac{(\chi_i^{\text{obs}} - \chi_i^{\text{calc}})^2}{(\chi_i^{\text{obs}})^2}\right]^{1/2} \qquad (3)$$

provides a measure of the goodness of fit. As seen from the F values and by visual inspection of the data compared to theory (Figure 7), the quality of the fits to theory is not affected significantly by the magnitude of the distortion parameters chosen for the octahedral metal centers and the g and J parameters obtained for the antiferromagnetically coupled centers are also relatively insensitive to the varying degrees of distortion chosen for the octahedral centers.

To put the magnitude of this antiferromagnetic coupling in perspective, we compare our results with those reported earlier for the closely related $[CuCl(imid)(imidH)_2]_x$, the structure of which consists of chains of copper ions bridged by imidazolate ligands.[14] The magnetic susceptibilities of the compound were fit to a linear chain model yielding $J = 84$ cm^{-1}.[15] The model employed in ref 15 used the Heisenberg spin Hamiltonian in the form $H = JS_1 \cdot S_2$; whereas the model employed in the present work has $H = -2JS_1 \cdot S_2$. Hence "J" $= -42$ cm^{-1} should be used for the copper(II) system in making comparisons with the current study. Moreover, to compare complexes with different total spin, S, it is appropriate to compare values of $|4JS^2|$ rather than J.[41] Employing $J = -2.3$ cm^{-1} for $[Fe_3(imid)_6(imidH)_2]_x$, $|4JS^2| = 37$ cm^{-1} for this compound compared to 42 cm^{-1} for the imidazolate-bridged copper(II) polymer. Interestingly, the value of $|4JS^2|$ for the previously studied imidazolate-bridged triangular complex, calculated as above for $[CuCl(imid)(imidH)_2]_x$,[17] is 38 cm^{-1}, in very close agreement with the other values. Clearly, the magnitude of the antiferromagnetic coupling in the extended chains of $[Fe_3(imid)_6(imidH)_2]_x$ is of the order expected for imidazolate-bridged metal ions.

The above analysis provides strong evidence for significant antiferromagnetic coupling between tetrahedral metal centers in $[Fe_3(imid)_6(imidH)_2]_x$. The magnetic phase transition at 17 K is consistent with long-range ordering at low temperatures. The observation of net magnetization at zero applied field below the transition temperature, combined with the fact that the maximum magnetization obtained falls considerably short of the theoretical saturation value, provides support for the conclusion that this is an example of canted spin antiferromagnetic coupling leading to weak ferromagnetism at low temperatures.[42] Support for a canted spin structure also comes from the X-ray-determined molecular structure which shows a systematic alternation of the relative orientation of the iron(II) chromophores along the imidazolate-bridged chains. As a measure of this, we calculated a dihedral angle of 43° between the vectors bisecting the N−Fe−N intrachain angles on adjacent tetrahedral iron atoms along the chain.

A previously reported canted spin iron(II) complex is $[Fe(4\text{-imidazoleacetate})_2]_x \cdot 2CH_3OH$.[43] The compound behaves magnetically as a 2-D antiferromagnetic system in which 3-D long-range ordering gives a net magnetic moment below 15 K. Magnetization experiments at 4.2 K on this compound revealed a coercive field of 6200 G and a remnant magnetization of 1200 cm^3 G mol^{-1}. In this system, the antiferromagnetic coupling occurs within sheets of octahedral iron(II) centers and hydrogen-bonding interactions between the sheets are presumed to promote the observed 3-D weak ferromagnetism. In contrast, in the system described in the present work, the antiferromagnetic coupling seems to occur in chains of tetrahedrally coupled iron(II) centers and coordinative links between these chains involving octahedral iron(II) centers promote 3-D order and weak ferromagnetism. More recently, the biimidazolate complex $[Fe(biimidazolate)]_x \cdot CH_3OH \cdot 0.5H_2O$[44] has been reported as another example of a canted spin iron(II) complex. Magnetic studies revealed a magnetic phase transition at 25 K, and magnetization data collected at 4.2 K again revealed a hysteresis loop with a reported coercive field of 2000 G and a remnant magnetization of 950 cm^3 G mol^{-1}. Unfortunately the structure of this compound has not been determined by single-crystal X-ray diffraction. Moreover, it should be noted that the structure proposed by the authors for the complex does not correlate with the empirical formula.

Acknowledgment. We thank the Natural Sciences and Engineering Research Council of Canada for financial support, P. Borda of this department for C, H, and N analyses, and C. J. Barbosa for experimental assistance.

Supporting Information Available: Lists of final atomic coordinates and equivalent isotropic thermal parameters, hydrogen atom parameters, anisotropic thermal parameters, torsion angles, nonbonded contacts, and least-squares planes (10 pages). See any current masthead page for ordering and Internet access instructions.

JA971558I

(40) Hiller, W.; Strahle, J.; Datz, A.; Hanack, M.; Hatfield, W. F.; Gutlich, P. *J. Am. Chem. Soc*. **1984**, *106*, 329−335.
(41) Lambert, S. L.; Hendrickson, D. N. *Inorg. Chem*. **1979**, *18*, 2683−2686.
(42) Kahn, O. *Molecular Magnetism*; VCH Publishers, Inc.: New York, 1993; p 322.
(43) Martinez-Lorente, M. A.; Petrouleas, V.; Poinsot, R.; Tuchagues, J. P.; Savariault, J. M.; Drillon, M. *Inorg. Chem.* **1991**, *30*, 3587−3589.
(44) Martinez-Lorente, M. A.; Dahan, F., Sanakis, Y.; Petrouleas, V.; Bousseksou, A.; Tuchagues, J. P. *Inorg. Chem*. **1995**, *34*, 5346−5357.